An Analysis and Design Framework for Robust Control of a Multi-Axis Active Vibration Isolation System with Unknown Payload

Wichaphon Fakkaew, Theeraphong Wongratanaphisan, Matthew O. T. Cole

Department of Mechanical Engineering, Chiang Mai University,
239 Huay Kaew Road, Muang, Chiangmai, 50200, Thailand.
Tel: 66 53 94 4146
email: *wong@dome.eng.cmu.ac.th*

Abstract

This paper presents a framework for model-based analysis of robust stability and performance for a multi-axis active vibration isolation system with constant but unknown payload and subject to modelling errors associated with structural flexibility. The theoretical treatment involves a linear time-invariant system subject to real parameter uncertainty associated with the unknown payload. A set of performance indices are formulated based on generalized $\mathcal{H}_2$ ($\mathcal{H}_g$) and $\mathcal{H}_\infty$ measures. A method for stability/performance verification is then developed using a parameter-dependent Lyapunov function that incorporates the kinetic energy of the uncertain payload mass. This allows nonconservative bounds on the performance indices to be established via numerical solution of a corresponding set of matrix inequalities. The approach is especially suitable, and computationally efficient, for multi-degree-of-freedom systems as the overall (symmetric positive-definite) properties of the system mass matrix are accounted for without involving information for each scalar parameter. The associated LMIs can therefore be solved in polynomial time with respect to the number of unknown parameters. Numerical examples for the case of sky-hook damping control and multi-objective $\mathcal{H}_g/\mathcal{H}_\infty$ control are provided that demonstrate the effectiveness of the method as a tool for model-based controller evaluation and multi-objective optimization.

Keywords: active vibration isolation, robust stability, structured uncertainty, LMI, multi-objective optimization

1 Introduction

Active vibration isolation systems (AVISs) are required to isolate precision instruments and processes from external vibration sources and are used in optical alignment, microscopic imaging, micro-manipulation, etc. Most AVISs designed to work with a range of payload masses use simple sky-hook damping control where higher gains are set for heavier payloads (Kerber et al., 2007). In principle, for a single-degree-of-freedom AVIS having a rigid platform, unlimited gain values can be used without risk of destabilisation. This is also true for a single-axis AVIS with continuous mass-spring support (Yan et al., 2010). In reality, however, the structure of an isolation platform does not behave as a rigid body, especially if its dimensions are large (Yoshioka et al., 2001). There may also exist some flexible components such as couplings between actuators and the system platform (Thayer et al., 1998). In these cases, the possibility of destablisation due to flexible mode dynamics becomes an important issue. Although, in practice, controller gains can be limited to avoid instability problems, a direct treatment of the issue within a controller design procedure is clearly desirable. More discussion on this topic can be found in (Kim et al., 2001; Brennan et al., 2007).

In robust controller design, the effects of structural flexibility can often be treated using frequency domain (non-parametric) uncertainty bounds. For a multi-axis AVIS, methods that deal directly with robustness to unknown payloads in conjunction with non-parametric model uncertainty have not been widely considered. A number of studies have addressed issues regarding uncertainty in the system mass parameters, e.g. via uncertain system state space matrices (Iwasaki and Shibata, 1999; Whorton, 2002). Explicit treatment of an uncertain mass matrix was considered in the design of an active seat suspension system (Maciejewski et al., 2010; Zhao et al., 2010). For a multi-axis AVIS, the problem is more complicated, and robust performance under large variations of many mass parameters has not been addressed. Specifically, there is a need to develop robust stability and performance criteria that can be used to assess control effectiveness in this situation and ultimately to synthesize or optimize controllers. This study focuses on the development of such criteria.

The remainder of the paper is organized as follows. In section 2, a model of an AVIS and its uncertainty is first defined. Controller design specifications are then formulated based on robust $\mathcal{H}_g$ and $\mathcal{H}_\infty$ norm-bound criteria. Corresponding model-based conditions involving matrix inequality constraints are presented in section 3. Numerical studies that demonstrate the effect of payload variation on controller performance are presented in section 4. The utility of the framework in assessing and optimizing controller designs is also shown. The final section draws conclusions.

2 System modeling and design specifications

2.1 System modeling

A linearized model of a multi-axis AVIS can be defined in the form

$$\left.\begin{array}{rcl} (M_N - \Delta)\ddot{\xi} + C\dot{\xi} + K(\xi - \xi_b) &=& C\dot{\xi}_b + Hu \\ y &=& F\ddot{\xi} \end{array}\right\} \tag{1}$$

where ξ, $\xi_b \in \mathbb{R}^n$ are payload and base displacements, respectively. The outputs $y \in \mathbb{R}^{n_s}$ are measurement signals from accelerometers (which are commonly used motion sensors in AVISs) while $u \in \mathbb{R}^{n_a}$ are control force inputs. $F \in \mathbb{R}^{n_s \times n}$ and $H \in \mathbb{R}^{n \times n_a}$ are transformation matrices

that map from the $n_s(\geq n)$ accelerometer axes and $n_a(\geq n)$ actuator axes, respectively, to the system coordinate axes. C and $K \in \mathbb{R}^{n\times n}$ are the damping and stiffness matrices, respectively. The mass matrix accounts for both the mass of the mobile plate and the expected mass of the payload. The nominal value M_N corresponds to the 'maximum' expected value so that the uncertainty $\Delta \in \mathbb{R}^{n\times n}$ takes constant positive semi-definite values. We may also write $M_N = M_0 + \bar{M}$ where M_0 corresponds to the mobile mounting plate and $\bar{M}$ is the maximum payload. For further analysis, the set of all possible payload uncertainty matrices is defined in the form

$$\mathcal{U}_\Delta = \left\{ \Delta \in \mathbb{R}^{n\times n} \,\middle|\, 0 \leq \Delta \leq \bar{M} \right\} \tag{2}$$

The system model will be subject to other errors arising, for example, due to unmodelled dynamics associated with mobile plate flexibility, flexibility in joints between the actuators and platform, sensors and/or actuators. These may be treated using standard multiplicative uncertainty representation where the open-loop transfer matrix from control input u to measured output y is expressed

$$G_{yu}(s,\, \Delta) = G_0(s,\, \Delta)\,(I + \Lambda W(s)) \tag{3}$$

where Λ is an operator representing the uncertainty. The transfer matrix $W(s)$ contains frequency-dependent normalizing factors (weighting functions) introduced such that $\|\Lambda\|_\infty \leq 1$ for all possible $\Delta \in \mathcal{U}_\Delta$. In practice, suitable weighting functions may be calculated according to the error between the (measured) frequency response of the actual system and that of the model. The nominal open-loop transfer matrix is given by.

To derive a state space model, we will first consider the term Δ in linear fraction transformation (LFT) form. Note that equation (1) can be written as

$$\ddot{\xi} = (M_N - \Delta)^{-1}\, f_T. \tag{4}$$

where $f_T = -C(\dot{\xi} - \dot{\xi}_b) - K(\xi - \xi_b) + Hu$. By defining p as reaction forces acting on the mobile platform due to the payload, equation (4) can alternatively be expressed

$$\ddot{\xi} = M_N^{-1}(f_T + p),\; p = \Delta\dot{q},\; q = \dot{\xi}. \tag{5}$$

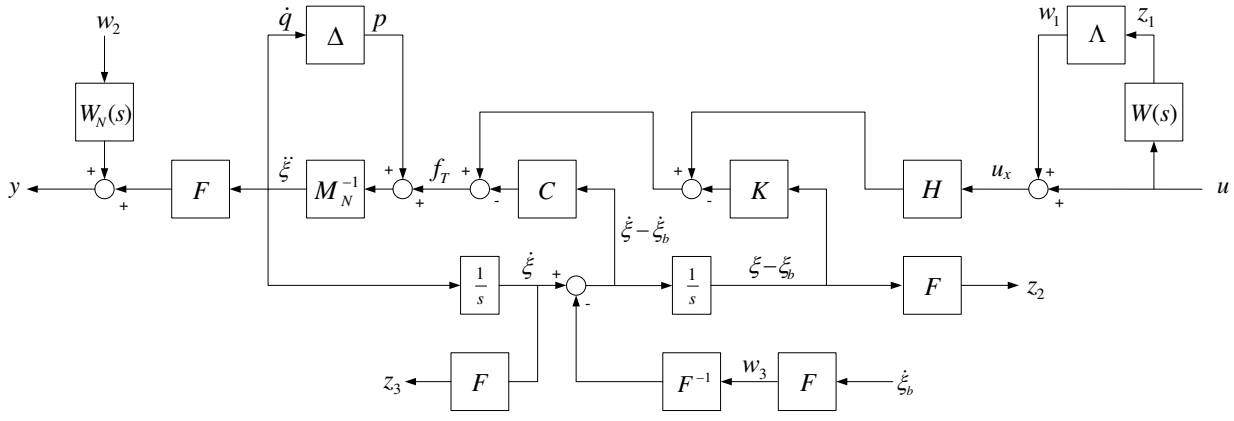

Figure 1: Block diagram of an AVIS including uncertainties

A block diagram for the system is shown in Figure 1. In this diagram, the system coordinates have been transformed to coincide with the sensor coordinates. Outputs are represented by z_i

and inputs represented by w_i, $i = 1, 2, 3$. The non-parametric uncertainties are captured through w_1, $z_1 \in \mathbb{R}^n$ while w_2, $z_2 \in \mathbb{R}^n$ represent sensor noise and payload-to-base relative displacement along sensor axes, respectively. w_3, $z_3 \in \mathbb{R}^n$ are, respectively, the velocities of the system base along sensor axes and the velocities of the payload. $W_N(s)$ is a weighting function used to model sensor noise.

Let $W(s)$ and $W_N(s)$ be defined in terms of state-space matrices: $W(s) = D_w + C_w(sI - A_w)^{-1}B_w$ and $W_N(s) = a_N I$, respectively. With state vector $x_G^T = \left[\ \dot{\xi}^T,\ \ \xi^T - \xi_b^T,\ \ x_3^T\ \right]$, where x_3 contains state variables for the weighting function $W(s)$, the complete state space model is given by

$$\left.\begin{array}{rcl} \dot{x}_G &=& Ax_G + B_0 p + B_1 w_1 + B_2 w_2 + B_3 w_3 + B_4 u \\ q &=& C_0 x_G \\ z_1 &=& C_1 x_G + D_{14} u \\ z_2 &=& C_2 x_G \\ z_3 &=& C_3 x_G \\ y &=& C_4 x_G + D_{40} p + D_{41} w_1 + D_{42} w_2 + D_{43} w_3 + D_{44} u \\ p &=& \Delta \dot{q},\ \Delta \in \mathcal{U}_\Delta \\ w_1 &=& \Lambda z_1,\ \|\Lambda\|_\infty \leq 1 \end{array}\right\} \tag{6}$$

where

$$\left[\begin{array}{cccccc} A & B_0 & B_1 & B_2 & B_3 & B_4 \\ C_0 & 0 & 0 & 0 & 0 & 0 \\ C_1 & 0 & 0 & 0 & 0 & D_{14} \\ C_2 & 0 & 0 & 0 & 0 & 0 \\ C_3 & 0 & 0 & 0 & 0 & 0 \\ C_4 & D_{40} & D_{41} & D_{42} & D_{43} & D_{44} \end{array}\right]$$

$$= \left[\begin{array}{ccc|c|c|c|c|c} -M_N^{-1}C & -M_N^{-1}K & 0 & M_N^{-1} & M_N^{-1}H & 0 & M_N^{-1}CF^{-1} & M_N^{-1}H \\ I & 0 & 0 & 0 & 0 & 0 & -F^{-1} & 0 \\ 0 & 0 & A_w & 0 & 0 & 0 & 0 & B_w \\ \hline I & 0 & 0 & 0 & 0 & 0 & 0 & 0 \\ \hline 0 & 0 & C_w & 0 & 0 & 0 & 0 & D_w \\ \hline 0 & F & 0 & 0 & 0 & 0 & 0 & 0 \\ \hline F & 0 & 0 & 0 & 0 & 0 & 0 & 0 \\ \hline -FM_N^{-1}C & -FM_N^{-1}K & 0 & FM_N^{-1} & FM_N^{-1}H & a_n I & F\ M_N^{-1}CF^{-1} & FM_N^{-1}H \end{array}\right]$$

Suppose that $(A,\ B_4)$ is controllable and $(A,\ C_4)$ is observable. Output feedback control of the system may then be achieved with a linear controller $K(s) = C_K\left(sI - A_K\right)^{-1} B_K$ realised as

$$\left.\begin{array}{rcl} \dot{x}_K &=& A_K x_K + B_K y \\ u &=& C_K x_K \end{array}\right\} \tag{7}$$

The overall system includes two separate feedback interconnections: one involving parametric uncertainty Δ and the other involving non-parametric uncertainty Λ (see Figure 2(a)). The closed loop system can be considered in the form shown in Figure 2(b) where parametric uncertainty is accounted for within the uncertain-parameter-dependent model $\mathcal{T}(s)$. Here, the controller and parametric uncertainty are embedded in $\mathcal{T}(s) = \mathcal{F}_u\left(\mathcal{F}_l(G(s),\ K(s)),\ s\Delta\right)$ where $\mathcal{F}_l\left(\cdot,\ \cdot\right)$ and $\mathcal{F}_u\left(\cdot,\ \cdot\right)$ represent a lower and upper linear fractional transformation (Doyle et al., 1991), respectively. The closed-loop subsystems $\mathcal{T}_{ii}$ $(i = 1, \ldots, 3)$ have the following state space

descriptions:

$$\mathcal{T}_{ii}: \begin{cases} \dot{x} &= \mathcal{A}x + \mathcal{B}_0 p + \mathcal{B}_i w_i \\ q &= \mathcal{C}_0 x \\ z_i &= \mathcal{C}_i x \\ p &= \Delta\dot{q},\ \Delta \in \mathcal{U}_\Delta \end{cases} \tag{8}$$

where $x = [x_G^T \quad x_K^T]^T \in \mathbb{R}^{n+n_k}$ and

$$\left[\begin{array}{c|c|c} \mathcal{A} & \mathcal{B}_0 & \mathcal{B}_i \\ \hline \mathcal{C}_0 & 0 & 0 \\ \hline \mathcal{C}_i & 0 & 0 \end{array}\right] = \left[\begin{array}{cc|c|c} A & B_4C_K & B_0 & B_i \\ B_KC_4 & A_K + B_KD_{44}C_K & B_KD_{40} & B_KD_{4i} \\ \hline C_0 & 0 & 0 & 0 \\ \hline C_i & D_{i4}C_K & 0 & 0 \end{array}\right].$$

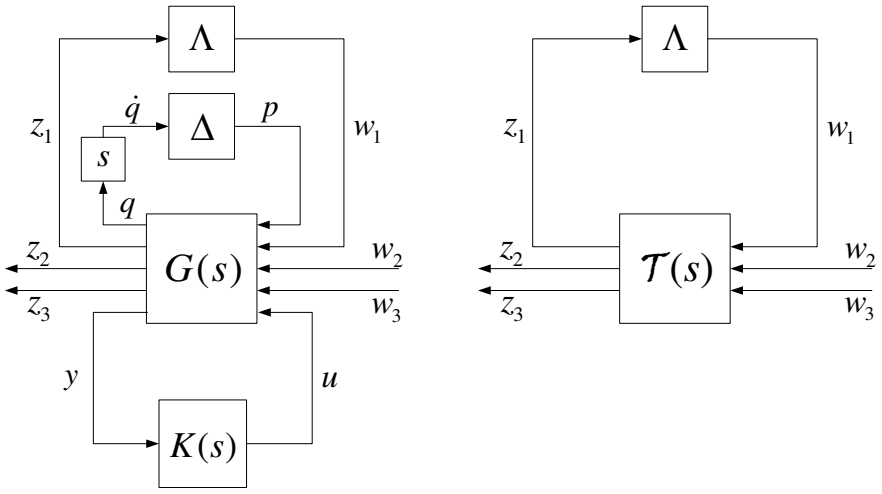

Figure 2: (a) Robust controller design framework, (b) Closed-loop system with non-parametric uncertainty

2.2 Robust stability and performance specifications

Robust stability

Robustness to model uncertainty can be enforced by a $\mathcal{H}_\infty$ norm-bound criterion for the uncertain-parameter-dependent subsystem $\mathcal{T}_{11}$. From Figure 2(b), the system is robustly stable for all uncertainties satisfying $\|\Lambda\|_\infty \leq 1$ if and only if (Zhou and Doyle, 1998)

$$\|\mathcal{T}_{11}\|_\infty < 1,\ \forall\Delta \in \mathcal{U}_\Delta. \tag{9}$$

Acconting for parametric uncertainty (unknown payload mass) in this criterion will be considered in detail in section 3.

Robust performance

For a single-axis AVIS, isolation performance is usually assessed in terms of *transmissibility*, which is the ratio of payload response amplitude to base motion amplitude under conditions of steady-state sinusoidal excitation. For a multi-axis AVIS, alternative measures must be considered that take account of all axes. Let $\mathcal{T}_{33}(s) \in \mathbb{C}^{n\times n}$ denote the transfer matrix from w_3 to z_3:

$$\tilde{z}_3(s) = \mathcal{T}_{33}(s)\tilde{w}_3(s). \tag{10}$$

For sinusoidal base excitation $w_3 = W_3 e^{j\omega t}, W_3 \in \mathbb{C}^n$, the steady-state response of the payload is $z_3(t) = Z_3(j\omega)e^{j\omega t}$ where

$$Z_3(j\omega) = \mathcal{T}_{33}(j\omega)W_3. \tag{11}$$

The frequency-dependent *effective transmissibility* may be defined in terms of a suitable norm of $\mathcal{T}_{33}(j\omega)$. In some previous studies, the Frobenius norm of $\mathcal{T}_{33}$ has been considered (Spanos et al., 1995; Thayer et al., 1998). This can be viewed as the root-mean-square value of all elements of the transmissibility matrix. An alternative performance measure may be defined as

$$\mathcal{T}_{eff}(\omega) = \bar{\sigma}\left(\mathcal{T}_{33}(j\omega)\right) \tag{12}$$

which is the worst-case transmissibility over all possible transmission directions.

Although the effective transmissibility is a useful measure of performance it must be evaluated point-wise over ω. The worst-case (maximum) value of $\mathcal{T}_{eff}(\omega)$ over all ω provides a useful scalar performance index and is equivalent to the $\mathcal{H}_\infty$ norm of $\mathcal{T}_{33}$. For controller design, it is also useful to consider a performance index that accounts for isolation performance over all frequencies. In some studies, a cost function for controller optimization has been defined in terms of the $\mathcal{H}_2$ norm of $\mathcal{T}_{33}$ (Thayer et al., 1998):

$$\|\mathcal{T}_{33}\|_2^2 = \mathbf{Tr}\left(\frac{1}{2\pi}\int_{-\infty}^{\infty}\mathcal{T}_{33}(j\omega)\mathcal{T}_{33}^*(j\omega)\,d\omega\right) \tag{13}$$

An alternative but closely related cost function is given by

$$\|\mathcal{T}_{33}\|_g^2 = \bar{\lambda}\left(\frac{1}{2\pi}\int_{-\infty}^{\infty}\mathcal{T}_{33}(j\omega)\mathcal{T}_{33}^*(j\omega)\,d\omega\right). \tag{14}$$

$\|\mathcal{T}_{33}\|_g$ is known as the *generalized* $\mathcal{H}_2$ norm of $\mathcal{T}_{33}$ (or $\mathcal{H}_g$ norm) (Rotea, 1993; Scherer et al., 1997). For the single-axis case, these two cost functions are equivalent and correspond to the total area under the plot of $\mathcal{T}_{eff}^2(\omega)$. For the multi-axis case, the two indices have slightly different physical interpretation as the $\mathcal{H}_2$ norm averages over all possible transmission directions whereas the $\mathcal{H}_g$ norm corresponds to the worst-case transmission direction. There is justification for using the $\mathcal{H}_g$ norm when there is likely to be a dominant direction for excitation. For many operating environments, this will be the case. If the dominant direction is not known in advance it then makes sense to optimize for the worst-case scenario. For environments where excitation may occur simultaneously in all directions, the $\mathcal{H}_2$ measure may be more appropriate. In this work we adopt the $\mathcal{H}_g$ norm for performance analysis, in correspondence with the first situation.

Design specifications

From the discussion of performance measures given previously, the following set of design specifications may be defined:

$$\left.\begin{array}{rcl} \|\mathcal{T}_{11}\|_\infty & < & 1 \\ \|\mathcal{T}_{22}\|_\infty & < & \gamma_2 \\ \|\mathcal{T}_{33}\|_\infty & < & \gamma_3 \\ \|\mathcal{T}_{33}\|_g^2 & < & \nu \end{array}\right\} \forall \Delta \in \mathcal{U}_\Delta \tag{15}$$

The first condition can be used to ensure that modelling error and neglected dynamics do not cause internal instability. The second condition is used to limit payload drift caused by sensor noise to within some specified level. This undesirable effect usually occurs for systems using accelerometer-based sensing if the controller gain is not limited in the low frequency range. The third condition limits the worst-case effective transmissibility, while the last condition may be used to optimize the isolation performance over the entire frequency range, as defined by equation (14).

3 Stability and performance analysis

This section considers the design specifications (15) and derives corresponding sufficient conditions from a Lyapunov stability/performance analysis. The analysis is applied to the state-space descriptions of the closed-loop subsystems (8) and leads to a set of LMI constraints, as given in the following theorem.

Theorem 1. *For the system in equation (8) with*

$$\mathbf{\Delta} = \left\{ \Delta \,|\Delta = \Delta^T \geq 0,\, \bar{\sigma}(\Delta) \leq \epsilon^{-1} \right\}, \tag{16}$$

the following conditions hold:
(i) $\|\mathcal{T}_{ii}\|_\infty < \gamma_i,\ i = 1,\, 2,\, 3\ \forall \Delta \in \mathbf{\Delta}$ *if there exist* $\mathcal{X}_i > 0$ *and scalars* $\beta_i > 0$, $\mu_i > 0$, $\pi_i > 0$ *satisfying*

$$\left[\begin{array}{cccc} \mathcal{A}^T\mathcal{X}_i + \mathcal{X}_i\mathcal{A} & \mathcal{X}_i\mathcal{B}_0 + \mathcal{C}_0^T\beta_i + \mathcal{A}^T\mathcal{C}_0^T\mu_i & \mathcal{X}_i\mathcal{B}_i & \mathcal{C}_0^T\pi_i \\ \mathcal{B}_0^T\mathcal{X}_i + \beta_i\mathcal{C}_0 + \mu_i\mathcal{C}_0\mathcal{A} & \mu_i(-2\epsilon I + \mathcal{B}_0^T\mathcal{C}_0^T + \mathcal{C}_0\mathcal{B}_0) & \mu_i\mathcal{C}_0\mathcal{B}_i & 0 \\ \mathcal{B}_i^T\mathcal{X}_i & \mathcal{B}_i^T\mathcal{C}_0^T\mu_i & -\gamma_i\pi_i I & 0 \\ \pi_i\mathcal{C}_0 & 0 & 0 & -\gamma_i\pi_i I \end{array}\right] < 0, \tag{17}$$

(ii) $\|\mathcal{T}_{33}\|_g^2 < \nu,\ \forall \Delta \in \mathbf{\Delta}$, *if there exist* $\mathcal{X}_g > 0$ *and scalar* $\mu_g > 0$ *satisfying*

$$\left[\begin{array}{ccc} \mathcal{A}^T\mathcal{X}_g + \mathcal{X}_g\mathcal{A} & \mathcal{X}_g\mathcal{B}_0 + \mathcal{C}_0^T\beta_g + \mathcal{A}^T\mathcal{C}_0^T\mu_g & \mathcal{X}_g\mathcal{B}_3 \\ \mathcal{B}_0^T\mathcal{X}_g + \beta_g\mathcal{C}_0 + \mu_g\mathcal{C}_0\mathcal{A} & \mu_g\left(-2\epsilon I + \mathcal{B}_0^T\mathcal{C}_0^T + \mathcal{C}_0\mathcal{B}_0\right) & \mu_g\mathcal{C}_0\mathcal{B}_3 \\ \mathcal{B}_3^T\mathcal{X}_g & \mathcal{B}_3^T\mathcal{C}_0^T\mu_g & -I \end{array}\right] < 0, \tag{18}$$

$$\left[\begin{array}{cc} \mathcal{X}_g & \mathcal{C}_3^T \\ \mathcal{C}_3 & \nu I \end{array}\right] > 0. \tag{19}$$

Proof. The constraint $0 \leq \Delta = \Delta^T \leq \frac{1}{\epsilon} I$ is equivalent to $\epsilon\Delta^T\Delta \leq \Delta$ (Bernstein et al., 1995). Hence,

$$2\epsilon\Delta^T\Delta - \Delta^T - \Delta \leq 0. \tag{20}$$

Pre- and post-multiplying inequality (20) by $\dot{q}^T$ and $\dot{q}$, respectively, and applying $p = \Delta\dot{q}$ yields

$$2\epsilon p^T p - p^T\dot{q} - \dot{q}^T p \leq 0. \tag{21}$$

Consider a parameter-dependent Lyapunov function with the form

$$\mathcal{V}_i(x) = x^T\mathcal{X}_i x + \beta_i x^T\mathcal{C}_0^T\Delta\mathcal{C}_0 x,\ \forall\Delta\in\mathbf{\Delta},\ i=1,\,2,\,3,\,g \tag{22}$$

where $\mathcal{X}_i = \mathcal{X}_i^T$ and $\beta_i > 0$. Noting that $\mathcal{C}_0 x = \dot{\xi}$ is the velocity of the payload, the second term in $\mathcal{V}_i(x)$ corresponds to the kinetic energy of the payload. For $x \neq 0$, the condition $\mathcal{X}_i > 0$ suffices to ensure that $\mathcal{V}_i(x) > 0,\ \forall\Delta\in\mathbf{\Delta}$. Differentiating equation (22) and substituting $\Delta\mathcal{C}_0\dot{x} = \Delta\dot{q} = p$ yields

$$\dot{\mathcal{V}}_i(x) \;=\; \dot{x}^T\mathcal{X}_i x + x^T\mathcal{X}_i\dot{x} + \beta_i\left(p^T\mathcal{C}_0 x + x^T\mathcal{C}_0^T p\right). \tag{23}$$

(i) The condition $\|\mathcal{T}_{ii}\|_\infty < \gamma_i,\ \forall\Delta\in\mathbf{\Delta}$ holds if there exists a Lyapunov function $\mathcal{V}_i(x) > 0$ and a positive real scalar $\pi_i > 0$ such that (Boyd et al., 1994)

$$\dot{\mathcal{V}}_i(x) + \pi_i\left(\frac{1}{\gamma_i}z_i^T z_i - \gamma_i w_i^T w_i\right) < 0, \tag{24}$$

for all x, p, w satisfying the constraint (21). By the $\mathcal{S}$-procedure, this statement is equivalent to: there exists $\mathcal{V}_i(x) > 0$, $\pi_i > 0$, $\mu_i > 0$ such that

$$\dot{\mathcal{V}}_i(x) + \pi_i\left(\frac{1}{\gamma_i}z_i^T z_i - \gamma_i w_i^T w_i\right) - \mu_i(2\epsilon p^T p - p^T\dot{q} - \dot{q}^T p) \;<\; 0. \tag{25}$$

Substituting equations (23) and (8) into inequality (25), rearranging and using Schur complements yields the inequality (17).

(ii) The condition $\|\mathcal{T}_{33}\|_g^2 < \nu\ \forall\Delta\in\mathbf{\Delta}$ holds if there exists a Lyapunov function $\mathcal{V}_g(x) > 0$ such that

$$\mathcal{V}_g(x) - z_3^T Q^{-1} z_3 \;>\; 0, \tag{26}$$

$$\dot{\mathcal{V}}_g(x) - w_3^T w_3 \;<\; 0 \tag{27}$$

for all x, p, w satisfying the constraint (21) where $Q = Q^T > 0$. Refer to Appendix C for further explanation of these conditions. Assigning $Q^{-1} = \nu^{-1}I + \beta_g F^{-T}\Delta F^{-1}$, and applying the $\mathcal{S}$-procedure, we may conclude that $\|\mathcal{T}_{33}\|_g^2 < 1/\bar{\lambda}\left(\nu^{-1}I + \beta_g F^{-T}\Delta F^{-1}\right) < \nu,\ \forall\Delta\in\mathbf{\Delta}$ if there exists $\mathcal{V}_g(x) > 0$, $\mu_g > 0$ such that

$$\mathcal{V}_g(x) - z_3^T\left(\nu^{-1}I + \beta_g F^{-T}\Delta F^{-1}\right) z_3 \;>\; 0, \tag{28}$$

$$\dot{\mathcal{V}}_g(x) - w_3^T w_3 - \mu_g(2\epsilon p^T p - p^T\dot{q} - \dot{q}^T p) \;<\; 0 \tag{29}$$

Substituting equation (23) into inequality (29) yields inequality (18). Since $F^{-1}\mathcal{C}_3 = \mathcal{C}_0$, substituting equation (22) into equation (28) and simplifying yield $x^T\left(\mathcal{X}_g - \nu^{-1}\mathcal{C}_3^T\mathcal{C}_3\right)x > 0$. By Schur complements, this condition is equivalent to inequality (19).

Using the eigenvalue decomposition $F^{-T}\Delta F^{-1} = V\Psi V^T$ where $VV^T = I$, $\Psi = \mathrm{diag}(\psi_1,\,\psi_2,\,...,\,\psi_6)$, $\psi_1 \geq ... \geq \psi_6 \geq 0$, it follows that $\nu^{-1}I + \beta_g F^{-T}\Delta F^{-1} = \nu^{-1}V\Xi V^T$ where $\Xi = \mathrm{diag}(\tau_1,\,\tau_2,\,...,\,\tau_6)$, $\tau_i = 1 + \nu\beta_g\psi_i$. Note that $\psi_1 = \bar{\lambda}\left(F^{-T}\Delta F^{-1}\right) = \epsilon^{-1}\bar{\lambda}\left(F^{-T}F^{-1}\right)$. Hence,

$$\bar{\lambda}\left(\nu^{-1}I + \beta_g F^{-T}\Delta F^{-1}\right) \;=\; \nu^{-1}\left(1 + \nu\beta_g\epsilon^{-1}\bar{\lambda}\left(F^{-T}F^{-1}\right)\right). \tag{30}$$

It then follows that $\|\mathcal{T}_{33}\|_g < \nu\left(1 + \nu\beta_g\epsilon^{-1}\bar{\lambda}\left(F^{-T}F^{-1}\right)\right)^{-1} < \nu,\ \forall\Delta\in\mathbf{\Delta}$, as stated. □

Remarks

Remark 1 Theorem 1 provides a means to calculate $\mathcal{H}_\infty$ and $\mathcal{H}_g$ norm-bounds for the uncertain system with $0 \leq \Delta = \Delta^T \leq \epsilon^{-1} I$. A more general sector condition $M_1 \leq \Delta \leq M_2$, where M_1 and M_2 are symmetric positive definite matrices, could be handled by a loop-shifting transformation (Bernstein et al., 1995). For the current case, $\mathcal{U}_\Delta \subset \mathbf{\Delta}$ if $\bar{M} \leq \epsilon^{-1} I$. Consequently, if the conditions $\|\mathcal{T}_{ii}\|_\infty < \gamma_i,\ i = 1, 2, 3$ and $\|\mathcal{T}_{33}\|_g^2 < \nu$ hold for all $\Delta \in \mathbf{\Delta}$ then they also hold for all $\Delta \in \mathcal{U}_\Delta$.

Remark 2 Theorem 1 can be used for assessing robust stability and performance for a given system model by using standard LMI solvers. There are two approaches for testing whether $\|\mathcal{T}_{11}\|_\infty < 1$. One way is to set $\gamma_1 = 1$ and numerically test the feasibility of inequality (17). Another way is to solve the problem of minimizing γ_1 subject to inequality (17) where $i = 1$. If $\gamma_1 < 1$ is obtained, the system is robustly stable. These same tests can also be applied to evaluate whether $\|\mathcal{T}_{22}\|_\infty < \gamma_2$. For transmissibility evaluation, the overall performance can be obtained by minimizing ν subject to inequalities (18) and (19). Alternatively, a tighter upper bound for $\|\mathcal{T}_{33}\|_g^2$ can be obtained by assigning $\nu = \beta_g^{-1}$ and the overall performance can be obtained by maximizing β_g subject to inequalities (18) and

$$\begin{bmatrix} \mathcal{X}_g & \mathcal{C}_3^T \beta_g \\ \beta_g \mathcal{C}_3 & \beta_g I \end{bmatrix} > 0. \tag{31}$$

In addition, the worst-case transmissibility can be estimated by minimizing γ_3 subject to inequality (17) where $i = 3$. In each case, the optimization gives upper bounds for the performance indices.

Remark 3 Theorem 1 can also be applied in the synthesis of robust controllers satisfying the design specifications (15). Since inequalities (17) and (18) involve products of $\mathcal{X}_i$ and the controller matrix variables, the corresponding multi-objective controller synthesis problem will be non-convex. With some compromise, however, convexity can be enforced by seeking a common solution

$$\mathcal{X}_1 = \mathcal{X}_2 = \mathcal{X}_3 = \mathcal{X}_g = \mathcal{X} \tag{32}$$

to the constraints (17) - (19). This approach has been widely used in multi-objectives output feedback synthesis. A systematic procedure to turn non-convex constraints into LMI constraints or BLMI constraints on the synthesis variables can be consulted in (Scherer et al., 1997). A simple method to solve BLMIs in a control synthesis routine is to use an iteration scheme (Apkarian and Adams, 1998). To begin the iterations, some initial stabilizing controller that satisfies a sub-optimal set of design constraints (32) must be found.

Remark 4 To make some general comparisons with alternative approaches, consider the conventional LFT representation of uncertainty for the AVIS model (8)

$$\begin{aligned} \dot{x} &= \mathcal{A}x + \mathcal{B}_0 p + \mathcal{B}_i w_i, \\ r &= \dot{q} = \tilde{\mathcal{C}}_0 x + \tilde{\mathcal{D}}_{00} p + \tilde{\mathcal{D}}_{0i} w_i, \\ p &= \Delta r,\ \Delta \in \mathcal{U}_\Delta \end{aligned}$$

where $\tilde{\mathcal{C}}_0 = \mathcal{C}_0 \mathcal{A}$, $\tilde{\mathcal{D}}_{00} = \mathcal{C}_0 \mathcal{B}_0$ and $\tilde{\mathcal{D}}_{0i} = \mathcal{C}_0 \mathcal{B}_i$. Note that, in this form, the uncertainty has full-block form. Also, the plant has direct feed-through from p to r and so conventional

robust stability criteria for real parameter uncertainty, such as the multivariable Popov criterion (Bernstein et al., 1995), cannot be readily applied. An alternative approach, well-suited to LMI methods, is to treat Δ as the convex hull of a finite number of pre-specified matrices, i.e. $\Delta = \sum_i \alpha_i \Delta_i$, $\sum_i \alpha_i = 1$, where $\alpha_i > 0$ and Δ_i are the vertex values of Δ (Iwasaki and Shibata, 2001; Scherer, 1999). Unfortunately, computation time for the associated LMIs will increase exponentially with the number of uncertain elements of Δ. A similar approach involving a parameter-dependent Lyapunov function has been proposed for gain scheduled control where a single uncertain mass parameter could be measured/estimated on-line (Gao et al., 2006). In situations where there are a large number of uncertain mass parameters, these approaches tend to suffer from high computational complexity and increased conservativeness when compared with the method proposed in this paper.

4 Numerical case studies

In this section, application of the design criteria (through Theorem 1) will be demonstrated with numerical examples. For ease of explanation and comparison, a two-degrees-of-freedom (2-DOF) vibration isolator will be considered. Note, however, that the criteria can be applied to general multi-DOF systems.

4.1 Two-degrees-of-freedom vibration isolator

Consider the 2-DOF vibration isolator shown in Figure 3. The system consists of two active suspension units (ASUs), each comprising a spring, damper and actuator installed in parallel. A rigid platform which supports the payload is connected to the ASUs via flexible hinges. These flexible hinges allow the platform to pivot. The platform can, therefore, translate in the vertical direction and rotate. k_0 and c_0 represent the stiffness and damping of the springs in the ASUs. Two accelerometers measure platform accelerations y_1 and y_2 at their attachment points. k_1 and k_2 are the axial stiffness of the flexible hinges, which are high compared with the stiffness of the main support springs in the ASUs. m_1 and m_2 are the armature and stator masses of the actuators. m_0 and m_L are mobile plate mass and payload mass. I_0 and I_L are moments of inertia of the mobile plate and payload about the reference point. The case studies were undertaken for $m_0 = 10\,\text{kg}$, $m_1 = 0.1\,\text{kg}$, $m_2 = 0.4\,\text{kg}$, $I_0 = 0.3423\,\text{kg.m}^2$, $L = 0.25\,\text{m}$, $c_0 = 15\,\text{Ns/m}$, $k_0 = 12.5\,\text{kN/m}$ and $k_1 = k_2 = 1000\,\text{kN/m}$. The state-space description of the system is given in Appendix B.

A simplified model which does not include the effects of hinge flexibility will be used to design all controllers discussed. Hence, the mass of the actuator's armature can be lumped with the platform mass. The mass matrix is given by

$$M_0 = \begin{bmatrix} \frac{1}{4}m_e + \frac{1}{4L^2}I_e & \frac{1}{4}m_e - \frac{1}{4L^2}I_e \\ \frac{1}{4}m_e - \frac{1}{4L^2}I_e & \frac{1}{4}m_e + \frac{1}{4L^2}I_e \end{bmatrix} \tag{33}$$

where $m_e = m_0 + 2m_1$ and $I_e = I_0 + 2m_1L^2$, $C = \text{diag}(c_0, c_0)$, $K = \text{diag}(k_e, k_e)$, $k_e = k_0k_1k_2/(k_0k_1 + k_0k_2 + k_1k_2)$. The payload mass matrix is given by

$$M_L = \frac{1}{4}m_L \begin{bmatrix} 1 + (r/L)^2 & 1 - (r/L)^2 \\ 1 - (r/L)^2 & 1 + (r/L)^2 \end{bmatrix} \tag{34}$$

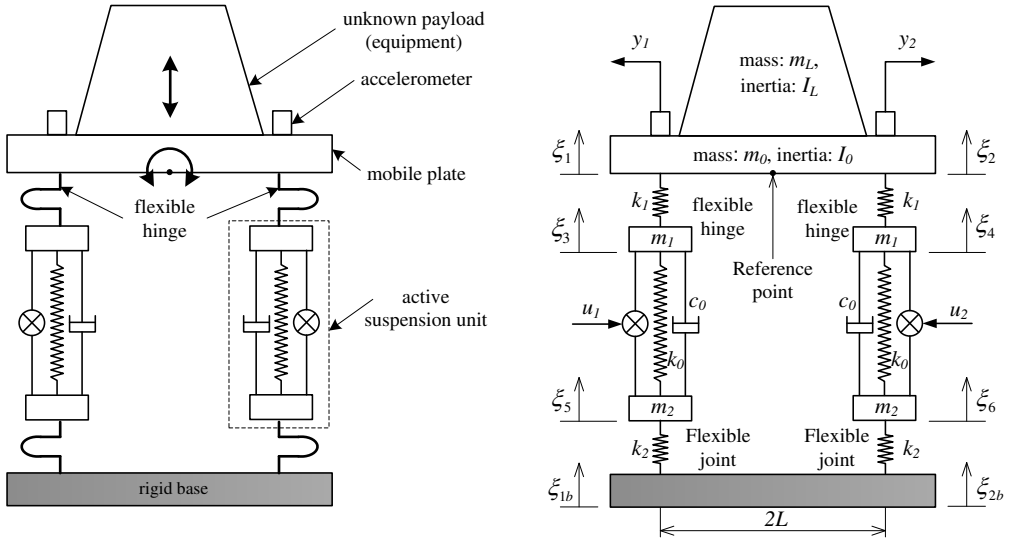

Figure 3: a) A 2-DOF AVIS with unknown payload b) Model used in case studies.

where m_L and r are the mass and radius of gyration of the payload. The maximum values of m_L, r and corresponding payload mass matrix are denoted by $\bar{m}_L$, $\bar{r}$ and $\bar{M}$, respectively. The parametric uncertainty is then given by

$$\Delta = \bar{M} - M_L. \tag{35}$$

It will be supposed also that the system is designed to support payloads up to 50 kg, i.e., $0 \leq m_L \leq 50\,\text{kg}$ and the mass distribution of the payload can vary such that $0 \leq r/L \leq 1$.

The effect of the hinge flexibility can be seen in Figure 4, which shows the maximum singular value plot for the simplified model $G_0(s, \Delta)$ (as used for controller design) compared with the complete model $G_{yu}(s, \Delta)$. The singular values match well in the low frequency range but differ significantly close to the natural frequencies associated with flexibility of the hinges. Figure 5 shows singular value plots for the multiplicative model error $\Lambda W(j\omega) = G_0^{-1}(j\omega, \Delta)G_{yu}(j\omega, \Delta) - I$ for various payload values. These plots are almost superimposed, indicating that mass variation does not greatly affect the multiplicative model error for the open-loop system. The weighting function $W(s) = \frac{22.5s^2+4241s+2.0\times10^5}{s^2+2827s+7.994\times10^6} I$ is selected as an upper bound for the model error so that $\|\Lambda\|_\infty \leq 1$ for all $\Delta \in \mathcal{U}_\Delta$ (over the range of payload mass). The sensor noise weighting function was selected as $W_N = a_n I$ where $a_n = 0.01$ m/s^2 is the estimated maximum accelerometer noise level. Supposing that the payload drift due to sensor noise is not to exceed 15 μm then this requires that $\|\mathcal{T}_{22}\| < 0.0015$ m/(m/s^2).

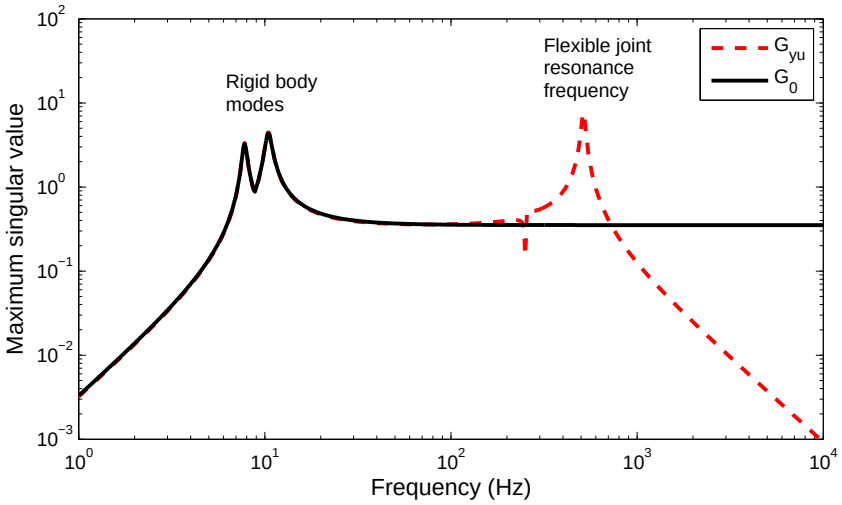

Figure 4: Plots of the maximum singular values of the transfer matrices $G_{yu}(s)$ and $G_0(s)$ at no-load condition.

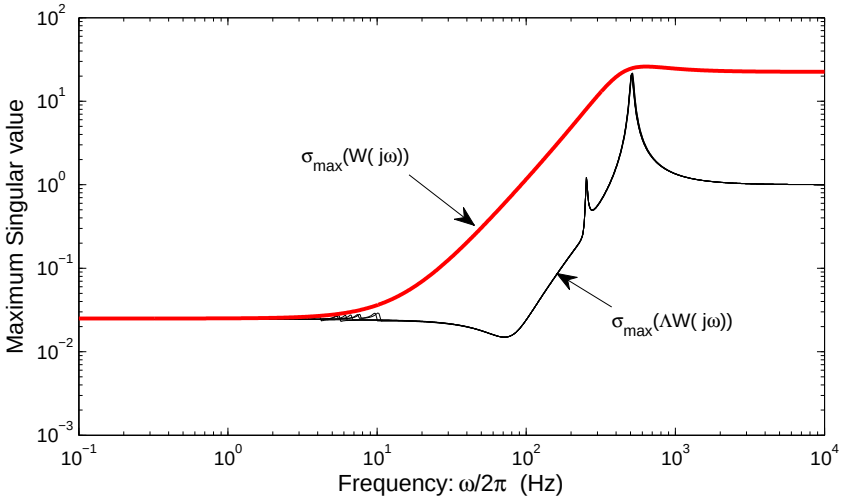

Figure 5: Weighting function $W(s)$ is selected as an upper-bound for the model error/uncertainty.

4.2 Controller designs

Acceleration-feedback controllers will be considered in the form

$$\tilde{u}(s) = K(s)\tilde{y}(s), \tag{36}$$

Four controller designs will be examined, which are 1) decentralized sky-hook damping with low gain, 2) decentralized sky-hook damping with high gain, 3) standard multi-objective $\mathcal{H}_g/\mathcal{H}_\infty$ controller and 4) multi-objective $\mathcal{H}_g/\mathcal{H}_\infty$ controller with robustness to payload uncertainty, as developed in this study.

a. Decentralized sky-hook damping control

A sky-hook damping controller, including conditioning filters, can be expressed

$$K(s) = \frac{s}{s+a} \cdot \frac{1}{s} \cdot \mathbf{K} = \frac{1}{s+a} \cdot \mathbf{K}$$

High-pass filters with cut-off frequency a are used to lessen the effects of low frequency drift. The gain matrix $\mathbf{K}$ can be selected to achieve the desired level of performance. Two decentralized sky-hook-damper controllers with different gains are considered: $K_1(s) = -\frac{1}{s+0.4}415I$ and $K_2(s) = -\frac{1}{s+0.4}650I$.

b. A multi-objective $\mathcal{H}_g/\mathcal{H}_\infty$ controller

This controller is designed with account of non-parametric uncertainty (due to hinge flexibility) but without regard to payload uncertainty. The nominal payload is selected as $m_L = 25$ kg, $r/L = 0.45$. The design specifications are set as to minimize $\|\mathcal{T}_{33}\|_g^2$ subject to $\|\mathcal{T}_{11}\|_\infty^2 < 1$ and $\|\mathcal{T}_{22}\|_\infty^2 < 0.0015$. The optimal controller is obtained from multi-objective output-feedback controller synthesis via LMI optimization (Scherer et al., 1997). The state space description of the optimized controller is

$$K_3 = \left[\begin{array}{cccccccc|cc}
-1.897 & -0.000 & -3.012 & 0.002 & -0.819 & -0.0000 & -32.30 & -0000 & -39.07 & 39.07 \\
0.000 & -1.846 & 0.003 & 3.824 & 0.000 & -1.339 & -0.011 & 0.375 & 38.32 & 38.32 \\
3.012 & -0.003 & -251.5 & -0.146 & -125.2 & 0.182 & -5577 & -0.061 & 30.90 & -30.84 \\
-0.002 & -3.824 & -0.119 & -460.5 & -0.014 & 355.3 & 6.760 & -90.87 & 39.50 & 39.54 \\
0.819 & 0.000 & -125.2 & 0.155 & -194.0 & 0.018 & -21543 & -0.094 & 8.426 & -8.431 \\
0.000 & -1.339 & -0.190 & -355.3 & 0.239 & -647.5 & -16.059 & 352.7 & 13.90 & 13.91 \\
-32.31 & -0.002 & 5577 & -4.430 & 21543 & 0.853 & -1046000 & 4.162 & -332.7 & 332.7 \\
0.001 & 0.375 & -0.023 & 90.87 & -0.293 & 352.7 & 34.07 & -1850 & -3.885 & -3.895 \\
\hline
39.07 & -38.32 & 30.90 & 39.50 & 8.433 & -13.90 & 332.6 & 3.890 & 0 & 0 \\
-39.07 & -38.32 & -30.84 & 39.54 & -8.424 & -13.91 & -332.8 & 3.890 & 0 & 0
\end{array}\right]. \quad (37)$$

c. A multi-objective $\mathcal{H}_g/\mathcal{H}_\infty$ controller with payload uncertainty robustness

For this controller, the design specifications are expressed by LMIs (17) - (19) with the maximum payload set at $\bar{m}_L = 50\,\text{kg}$ and $\bar{r}/L = 1$. (this means $\epsilon^{-1} = \bar{\sigma}(\bar{M}) = 25$.) This controller minimizes ν subject to LMIs (17) - (19) where $\gamma_1 = 1$ and $\gamma_2 = 0.0015$. The iteration starts with some stabilizing controller (in this case $K(s) = -\frac{1}{s+0.195}350I$) to obtain initial parameters for the optimization. The state space description of the optimized controller is

$$K_4 = \left[\begin{array}{cccccccc|cc} -1.089 & -0.000 & -0.985 & -0.006 & 1.559 & 0.039 & -7.793 & -0.082 & 29.11 & -29.16 \\ 0.000 & -1.827 & 0.042 & 3.408 & -0.004 & -0.157 & -0.614 & 1.405 & 30.93 & 30.88 \\ 0.985 & -0.019 & -11.24 & -1.443 & 34.18 & 0.963 & -181.7 & -2.475 & -12.77 & 13.09 \\ 0.005 & -3.408 & -0.513 & -494.3 & 3.457 & 42.72 & 172.7 & -417.7 & 28.70 & 28.77 \\ -1.559 & -0.001 & 34.19 & -0.600 & -486.1 & -26.48 & 5185 & 53.70 & 20.83 & -20.85 \\ 0.026 & 0.163 & -0.573 & 44.67 & 19.15 & -18.56 & 648.2 & 438.3 & -1.722 & -1.038 \\ -7.797 & -0.446 & 182.1 & -128.5 & -5188 & 421.0 & -197570 & -1460 & 108.0 & -100.6 \\ -0.065 & 1.407 & 1.747 & 418.3 & -42.25 & -435.8 & -722.0 & -4113 & -11.05 & -12.76 \\ \hline -29.10 & -30.94 & -12.56 & 28.68 & 20.78 & -0.811 & -109.4 & 10.80 & 0 & 0 \\ 29.18 & -30.87 & 13.29 & 28.78 & -20.90 & -1.839 & 99.22 & 12.97 & 0 & 0 \end{array}\right] \tag{38}$$

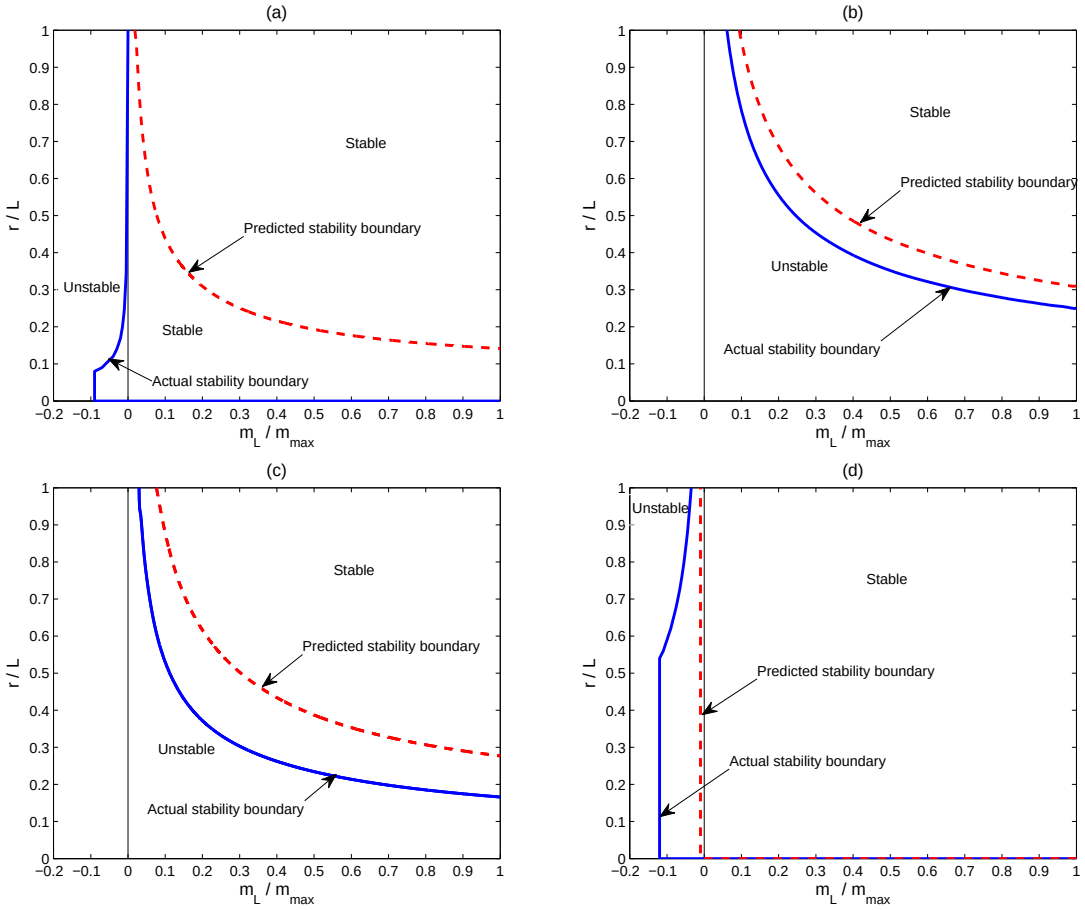

Figure 6: Stability map of the closed-loop system using controller (a) K_1, (b) K_2, (c) K_3 and (d) K_4.

4.3 Robustness and performance

Figure 6 shows the region of stability for each controller upon payload variation. Solid lines are actual stability boundaries while dashed lines are predicted boundaries obtained using Theorem 1

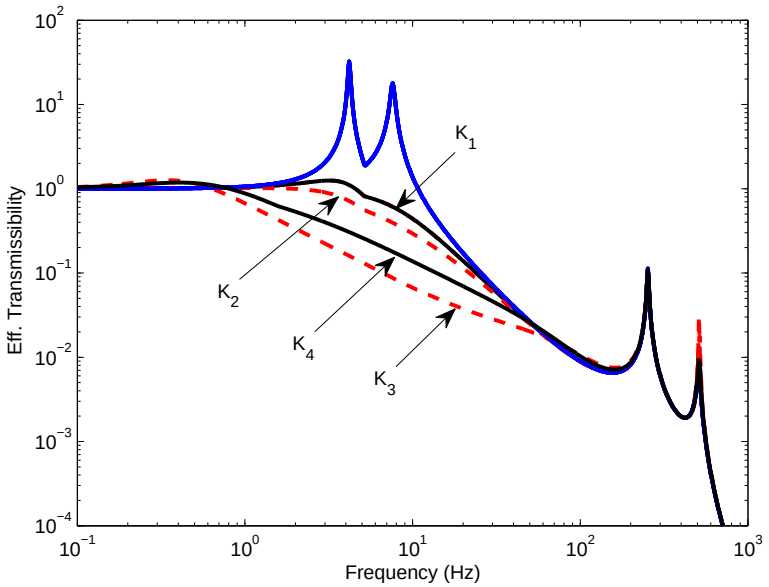

Figure 7: Effective transmissibility for $m_L = 25$ kg and $r/L = 0.45$.

(areas above the lines are stable). It can be observed that the predicted stability boundaries are reasonably close to the actual ones. Figure 7 shows the effective transmissibility of each controller for payload parameters $m_L = 25$ kg and $r/L = 0.45$. The decentralized sky-hook damping with low gain K_1 provides stable operation over the entire range of payloads. The higher-gain decentralized sky-hook damping K_2 gives better performance but destabilizes the system as the inertia of the payload decreases. The more sophisticated controller K_3 provides better performance when it is stable but cannot guarantee stability over the entire range of payloads. The controller K_4, designed for robustness to payload variation, provides stable operation over the entire payload range and achieves similar isolation performance to K_3.

Figure 8 shows simulated responses of the controlled systems under broad-band excitation at the base (the same set of excitation with velocity between -250 and 250 μm/s was used for all cases). The controllers were turned on after $t = 5$ sec. When the payload is set at $m_L = 25$ kg ($m_L/m_{Lmax} = 0.5$) and $r/L = 0.45$ (Figuer 8 (a)-(d)), all controllers provide stable isolation as predicted in the stability map (Figure 6). As expected, the higher-gain controller K_2 gives better performance than K_1 while K_3 and K_4 are comparatively superior. On the other hand, when m_L is decreased to 5.6 kg ($m_L/m_{Lmax} = 0.11$) systems controlled by K_2 and K_3 become unstable (Figure 8 (e)-(h)), consistent with the stability map. The performnace of K_4, in terms of transmitted vibration, is similar to when $m_L = 25$ kg.

Figure 9 shows the performance deterioration of each controller as the payload mass decreases (r/L remains fixed at 0.45). All controllers show little variation in performance (as evaluated by $\|\mathcal{T}_{33}\|_g$) except when the payload mass is close to the stability limit, where sudden degradation is observed. Both K_1 and K_4 give stable performance for all positive values of payload mass. Note, however, that if we extend the decrease in mass to negative values (implying physically that there is no payload and the mobile plate mass decreases) the system will reach an unstable condition. Clearly, K_4 is more robust to payload changes and has superior performance compared with the sky-hook damping controller K_1. A further general observation here is that increasing the payload inertia tends to have a stabilizing influence on the flexible mode dynamics.

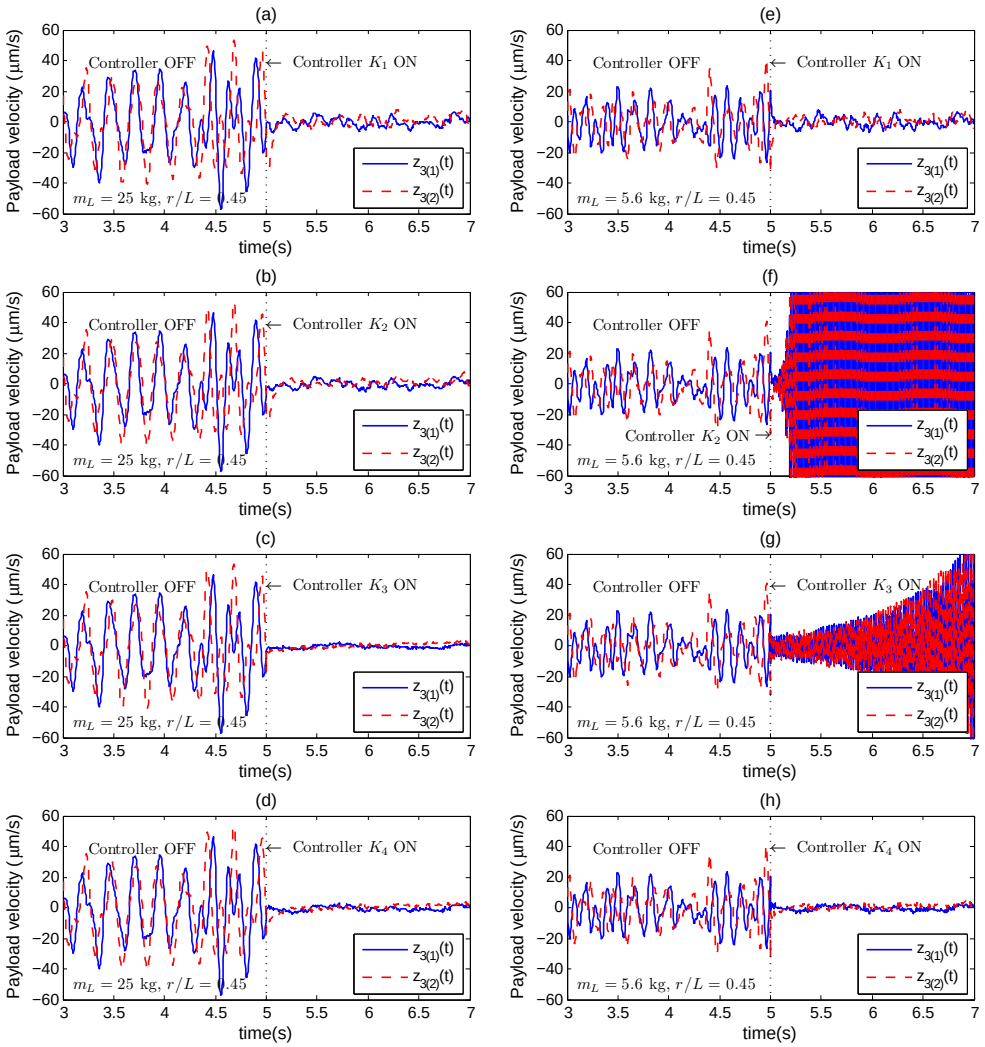

Figure 8: Simulated responses under broad-band excitation at the base (a) - (d) for $m_L = 25$ kg and $r/L = 0.45$ (e) - (h) for $m_L = 5.6$ kg and $r/L = 0.45$.

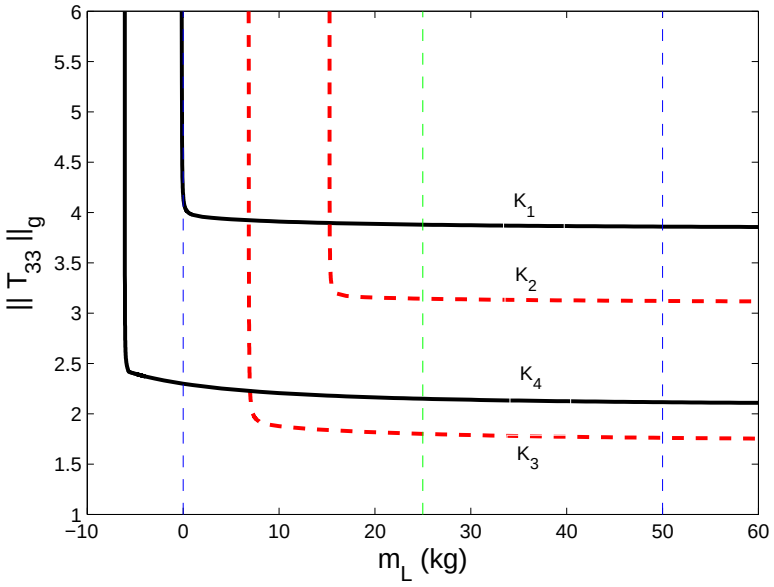

Figure 9: Performance deterioration as payload mass decreases.

5 Conclusions

A framework for model-based analysis of control performance for a multi-axis AVIS with unknown payload and subject to uncertain dynamics has been developed. Stability and performance specifications based on $\mathcal{H}_\infty$ and $\mathcal{H}_g$ norms of the system transfer functions have been proposed. Bounds on these norms can be established for the uncertain system via LMI constraints developed from a quadratic Lyapunov function incorporating the kinetic energy of the uncertain payload and with explicit account of the uncertainty structure for the payload mass matrix. Numerical results show that the stability boundaries predicted by this method are reasonably close to the actual boundaries, implying that the method is a good candidate among non-conservative analysis techniques for this type of problem. The method was further shown to be effective for multi-objective controller synthesis within an LMI framework, as good robust stability and performance could be attained.

Acknowledgment

This work has been financial supported by Thailand Research Fund and Office of the Higher Education Commission through the Royal Golden Jubilee Ph.D. Program [grant number PHD/0227/2550]; and NECTEC [grant number NT-B-22-E5-11-49-09].

References

Apkarian, P. and Adams, R. (1998). Advanced gain-scheduling techniques for uncertain systems. *IEEE Transactions on Control Systems Technology*, 6(1):21 –32.

Bernstein, D., Haddad, W., and Sparks, A. (1995). A Popov criterion for uncertain linear multivariable systems. *Automatica*, 31(7):1061 – 1064.

Boyd, S., El Ghaoui, L., Feron, E., and Balakrishan, V. (1994). *Linear Matrix Inequalities in Systems and Control Theory*. SIAM, Philadelphia.

Brennan, M., Ananthaganeshan, K., and Elliott, S. (2007). Instabilities due to instrumentation phase-lead and phase-lag in the feedback control of a simple vibrating system. *Journal of Sound and Vibration*, 304(3-5):466 – 478.

Doyle, J., Packard, A., and Zhou, K. (1991). Review of LFTs, LMIs, and μ;. In *Proceedings of the 30th IEEE Conference on Decision and Control*, pages 1227 –1232 vol.2.

Gao, H., Lam, J., and Wang, C. (2006). Multi-objective control of vehicle active suspension systems via load-dependent controllers. *Journal of Sound and Vibration*, 290(3 - 5):654 – 675.

Iwasaki, T. and Shibata, G. (1999). LPV system analysis via quadratic separator for uncertain implicit systems. In *Decision and Control, 1999. Proceedings of the 38th IEEE Conference on*, volume 1, pages 287 –292 vol.1.

Iwasaki, T. and Shibata, G. (2001). Lpv system analysis via quadratic separator for uncertain implicit systems. *IEEE Transactions on Automatic Control*, 46(8):1195 –1208.

Kerber, F., Hurlebaus, S., Beadle, B., and Stöbener, U. (2007). Control concepts for an active vibration isolation system. *Mechanical Systems and Signal Processing*, 21:3042–3059.

Kim, S., Elliott, S., and Brennan, M. (2001). Decentralized control for multichannel active vibration isolation. *IEEE Transactions on Control Systems Technology*, 9(1):93 –100.

Maciejewski, I., Meyer, L., and Krzyzynski, T. (2010). The vibration damping effectiveness of an active seat suspension system and its robustness to varying mass loading. *Journal of Sound and Vibration*, 329(19):3898 – 3914.

Rotea, M. (1993). The generalized H_2 control problem. *Automatica*, 29(2):373 – 385.

Scherer, C. (1999). *Advances in LinearMatrix Inequality Methods in Control, chapter 10*. SIAM, Philadelphia, Pa, USA.

Scherer, C., Gahinet, P., and Chilali, M. (1997). Multiobjective output-feedback control via LMI optimization. *IEEE Transactions on Automatic Control*, 42(7):896 –911.

Spanos, J., Rahman, Z., and Blackwood, G. (1995). A soft 6-axis active vibration isolator. *Proceedings of the American Control Conference*, 1:412–416.

Thayer, D., Campbell, M., and Vagners, J. (1998). Six axis vibration isolation using modern control techniques. *21st Annual AAS Guidance and Control Conference*, pages 1–15.

Whorton, M. (2002). Robust control for microgravity vibration isolation with parametric uncertainty. In *Proceedings of the American Control Conference*, pages 256–261.

Yan, B., Brennan, M., Elliott, S., and Ferguson, N. (2010). Active vibration isolation of a system with a distributed parameter isolator using absolute velocity feedback control. *Journal of Sound and Vibration*, 329(10):1601 – 1614.

Yoshioka, H., Takahashi, Y., Katayama, K., Imazawa, T., and Murai, N. (2001). An active microvibration isolation system for hi-tech manufacturing facilities. *Journal of Vibration and Acoustics*, 123(2):269–275.

Zhao, Y., Zhao, L., and Gao, H. (2010). Vibration control of seat suspension using H_∞ reliable control. *Journal of Vibration and Control*, 16(12):1859 – 1879.

Zhou, K. and Doyle, J. (1998). *Essentials of Robust Control.* Prentice-Hall.

Appendices

A Notation

$\mathbb{R}^n$ and $\mathbb{C}^n$	n-dimensional real and complex vectors, respectively
$\mathbb{R}^{m\times n}$ and $\mathbb{C}^{m\times n}$	real and complex $m \times n$ matrices, respectively.
I	identity matrix
diag(a_1, ..., a_n)	an $n \times n$ diagonal matrix with a_i as its ith diagonal element
A^T and A^*	transpose and complex conjugate transpose of A
A^{-1}	inverse of A
$\mathbf{Tr}(A)$	trace of A
$\lambda(A)$	eigenvalue of A
$\bar{\lambda}(A)$	maximum eigenvalue of A : $A = A^T \geq 0$
$\sigma(A)$ and $\bar{\sigma}(A)$	singular value and maximum singular value of A
$A < 0$ ($A \leq 0$)	A is a negative definite (semidefinite) matrix
$A > 0$ ($A \geq 0$)	A is a positive definite (semidefinite) matrix
$\tilde{x}(s)$	Laplace transform of signal x
$\tilde{x}(j\omega)$	Fourier transform of signal x

B Full model of a two-axis AVIS

Let $\xi_a^T = \begin{bmatrix} \xi_1 & \xi_2 & \xi_3 & \xi_4 & \xi_5 & \xi_6 \end{bmatrix}^T$, $z_3 = \dot{\xi}_a$, $\xi_b^T = \begin{bmatrix} \xi_{b1} & \xi_{b2} \end{bmatrix}^T$, $w_2 = \dot{\xi}_b$, $z_2 = \xi_r = \xi_a - L_a\xi_b$, where $L_a^T = \begin{bmatrix} 1 & 0 & 1 & 0 & 1 & 0 \\ 0 & 1 & 0 & 1 & 0 & 1 \end{bmatrix}$, $u^T = \begin{bmatrix} u_1 & u_2 \end{bmatrix}^T$, $y^T = \begin{bmatrix} y_1 & y_2 \end{bmatrix}^T$ and $w_2^T = \begin{bmatrix} n_1 & n_2 \end{bmatrix}^T$. The system state space model is

$$\left[\begin{array}{c} \dot{\xi}_a \\ \dot{\xi}_r \\ \hline z_2 \\ \hline z_3 \\ \hline y \end{array}\right] = \left[\begin{array}{cc|c|c|c} -M_a^{-1}C_a, & -M_a^{-1}K_a & M_a^{-1}C_{ab} & 0 & M_a^{-1}H_a \\ I_6 & 0_6 & -L_a & 0 & 0 \\ \hline 0 & F_a & 0 & 0 & 0 \\ \hline F_a & 0 & 0 & 0 & 0 \\ \hline -F_aM_a^{-1}C_a, & -F_aM_a^{-1}K_a & F_aM_a^{-1}C_{ab} & 0.01I_2 & F_aM_a^{-1}H_a \end{array}\right] \left[\begin{array}{c} \xi_a \\ \xi_r \\ \hline w_2 \\ \hline w_3 \\ \hline u \end{array}\right]$$

where

$$M_a = \begin{bmatrix} M_0 + M_L & 0 \\ 0 & M_{22} \end{bmatrix},\ M_0 = \begin{bmatrix} \frac{1}{4}m_0 + \frac{1}{4L^2}I_0 & \frac{1}{4}m_0 - \frac{1}{4L^2}I_0 \\ \frac{1}{4}m_0 - \frac{1}{4L^2}I_0 & \frac{1}{4}m_0 + \frac{1}{4L^2}I_0 \end{bmatrix},$$

$$M_{22} = \begin{bmatrix} m_1 & 0 & 0 & 0 \\ 0 & m_1 & 0 & 0 \\ 0 & 0 & m_2 & 0 \\ 0 & 0 & 0 & m_2 \end{bmatrix},\ C_a = \begin{bmatrix} 0 & 0 & 0 & 0 & 0 & 0 \\ 0 & 0 & 0 & 0 & 0 & 0 \\ 0 & 0 & c_0 & 0 & -c_0 & 0 \\ 0 & 0 & 0 & c_0 & 0 & -c_0 \\ 0 & 0 & -c_0 & 0 & c_0 & 0 \\ 0 & 0 & 0 & -c_0 & 0 & c_0 \end{bmatrix},$$

$$K_a = \begin{bmatrix} k_1 & 0 & -k_1 & 0 & 0 & 0 \\ 0 & k_1 & 0 & -k_1 & 0 & 0 \\ -k_1 & 0 & k_0 + k_1 & 0 & -k_0 & 0 \\ 0 & -k_1 & 0 & k_0 + k_1 & 0 & -k_0 \\ 0 & 0 & -k_0 & 0 & k_0 + k_2 & 0 \\ 0 & 0 & 0 & -k_0 & 0 & k_0 + k_2 \end{bmatrix},$$

$$F_a = \begin{bmatrix} 1 & 0 \\ 0 & 1 \\ 0 & 0 \\ 0 & 0 \\ 0 & 0 \\ 0 & 0 \end{bmatrix}^T,\ C_{ab} = \begin{bmatrix} 0 & 0 \\ 0 & 0 \\ 0 & 0 \\ 0 & 0 \\ 1 & 0 \\ 0 & 1 \end{bmatrix},\ H_a = \begin{bmatrix} 0 & 0 \\ 0 & 0 \\ 1 & 0 \\ 0 & 1 \\ -1 & 0 \\ 0 & -1 \end{bmatrix},$$

C Calculation of bounds on $\mathcal{H}_2$ and $\mathcal{H}_g$ norms

Consider a stable LTI system $\dot{x} = Ax + Bw$, $z = Cx$. Let $G(s) = C(sI - A)^{-1}B$. It is well known that $\|G\|_2^2 = \mathbf{Tr}\left(CZ_0C^T\right)$ and $\|G\|_g^2 = \bar{\lambda}\left(CZ_0C^T\right)$ where $Z_0 = Z_0^T$ is the unique solution to $AZ_0 + Z_0A^T + BB^T = 0$. In addition, $\|G\|_2^2 < \mathbf{Tr}(Q)$ and $\|G\|_g^2 < \bar{\lambda}(Q)$ if there exists a Lyapunov function $V(x) = x^TXx > 0$ such that

$$V(x) - z^TQ^{-1}z > 0, \tag{C.1}$$

$$\dot{V}(x) - w^Tw < 0. \tag{C.2}$$

To show this, let $Z = Z^T > Z_0$ where Z satisfies

$$AZ + ZA^T + BB^T < 0. \tag{C.3}$$

With an auxiliary parameter $Q = Q^T > 0$ satisfying

$$CZC^T < Q, \tag{C.4}$$

it can be verified that $\|G\|_2^2 < \mathbf{Tr}(Q)$ and $\|G\|_g^2 < \bar{\lambda}(Q)$. Define a Lyapunov function $V(x) = x^TXx$ where $X = Z^{-1}$. Pre- and post-multiplying inequality (C.3) by Z^{-1} and applying Schur complement, yield

$$\begin{bmatrix} A^TX + XA & XB \\ B^TX & -I \end{bmatrix} < 0. \tag{C.5}$$

Pre- and post-multiply inequality (C.5) by $\begin{bmatrix} x^T & p^T \end{bmatrix}$ and $\begin{bmatrix} x^T & p^T \end{bmatrix}^T$, respectively, yield inequality (C.2). Substituting $Z = X^{-1}$ into inequality (C.4), yields $CX^{-1}C^T < Q$ which is also equivalent to $X - C^TQ^{-1}C > 0$ by Schur complement. Pre- and post-multiplying the results by x^T and x, respectively yield inequality (C.1).